Numerical simulation of the mechanical behavior of ultrafine- and coarse-grained Zr–Nb alloys over a wide range of strain rates

V. A. Serbenta, N. V. Skripnyak, V. A. Skripnyak, and E. G. Skripnyak

Citation: AIP Conference Proceedings **1909**, 020190 (2017);
View online: https://doi.org/10.1063/1.5013871
View Table of Contents: http://aip.scitation.org/toc/apc/1909/1
Published by the American Institute of Physics

Numerical Simulation of the Mechanical Behavior of Ultrafine- and Coarse-Grained Zr–Nb Alloys over a Wide Range of Strain Rates

V. A. Serbenta[1,a)], N. V. Skripnyak[1,2,b)], V. A. Skripnyak[1,c)], and E. G. Skripnyak[1,d)]

[1] *National Research Tomsk State University, Tomsk, 634050 Russia*
[2] *Linköping University, Sweden*

[a)] Corresponding author: serbenta3@mail.ru
[b)] natali.skrp@mail.ru
[c)] skrp2006@yandex.ru
[d)] skrp@ftf.tsi.ru

Abstract. This paper presents the results on the development of theoretical methods of evaluation and prediction of mechanical properties of Zr–Nb alloys over a range of strain rates from 10^{-3} to 10^{3} s^{-1}. The mechanical behavior of coarse- and ultrafine-grained Zr–1Nb (E110) was investigated numerically. The ranges of strain rates and temperatures in which the mechanical behavior of Zr–1Nb alloy can be described using modified models of Johnson–Cook and Zerilli–Armstrong were defined. The results can be used in engineering analysis of designed technical systems for nuclear reactors.

INTRODUCTION

The improvement of the fabrication technology of fuel claddings and some constructional elements of nuclear reactors is associated with the computer simulation of mechanical properties and structural evolution of radiation-resistant Zr–Nb alloys [1, 2]. In this regard, there is an increasing need to develop computational models of the mechanical behavior of advanced Zr–Nb in the loading conditions close to operating ones. Zr–Nb has a unique complex of physical and mechanical properties and is considered as a promising structural alloy for nuclear reactors of generation IV. Coarse-grained (CG) and ultrafine-grained (UFG) zirconium alloys with the Nb concentration below 2.5 wt % and additionally doped with Mo, Fe, Cr for the stabilization of Zr beta-phase precipitates have been studied during the last decade [3, 4]. It is known that the formation of UFG structures in Zr–Nb alloys not only improves the yield strength of the alloy, but also prevents the formation of cracks at the mesoscopic level [5, 6]. In this connection, the mechanical behavior of Zr–Nb alloys was studied by numerical simulation in the practically important temperature range from 297 to 1243 K.

COMPUTATIONAL MODEL

The computational model uses the theoretical basis of continuum damage mechanics [7]. Mechanical behavior was described by a system of conservation equations (mass, momentum and energy), a kinematic equation, and a constitutive equation. The initial and boundary conditions were added to the system of equations. The boundary conditions correspond to the conditions of loading of a 3D body. Dog-bone specimens were simulated under axial tension with a constant strain rate. Cylindrical specimens were simulated under axial compression with a constant strain rate. Computer simulations were performed with the use of licensed software ANSYS 14.5 and software AUTODYN.

Proceedings of the International Conference on Advanced Materials with Hierarchical Structure for New Technologies and Reliable Structures 2017 (AMHS'17)
AIP Conf. Proc. 1909, 020190-1–020190-4; https://doi.org/10.1063/1.5013871
Published by AIP Publishing. 978-0-7354-1601-7/$30.00

TABLE 1. Material parameters of the Johnson–Cook model for Zr–1Nb

a, MPa	k_h, MPa μm$^{1/2}$	b, MPa	n	m	c
290	368 for 1.1 μm < dg < 100 μm	386	0.11	0.6 at T < 1070 K	0.14
625	40 for 0.08 μm < dg < 1.1 μm	386	0.11	0.21 at T < 1070 K 0.14 at T > 1070 K	0.14

TABLE 2. Material parameters of the Zerilli–Armstrong model for Zr–1Nb

C_0, MPa	k_h, MPa μm$^{1/2}$	C_1, MPa	C_3, MPa	C_4, MPa	C_5, MPa	n_1
110	368 for 1.1 μm < dg < 100 μm	1015	0.00807 at T < 1070 K	0.000395	405	0.19
445	40 for 0.08 μm < dg < 1.1 μm	1015	0.00807 at T < 1070 K	0.000395	405	0.19

The calculations were carried out with solvers using a finite difference scheme of second-order accuracy, or the method of smoothed particle hydrodynamics. Plastic flow was described within the theory of Prandtl–Reuss with the von Mises criterion. The flow stress of zirconium alloys under loading has been described using a modification of the Johnson–Cook model (1) and the Zerilli–Armstrong model (2) [8, 9]

$$\sigma_s(\varepsilon, \dot{\varepsilon}, T) = (a + k_h d_g^{-1/2} + b(\varepsilon_{eq}^p)^n)(1 + c \ln(\dot{\varepsilon}_{eq}/\dot{\varepsilon}_0))(1 - \overline{T}^m), \quad (1)$$

$$\sigma_s = C_0 + k_h d_g^{-1/2} + C_1 \exp(-C_3 T + C_4 T \ln(\dot{\varepsilon}_{eq}/\dot{\varepsilon}_0)) + C_5(\varepsilon_{eq}^p)^{n_1}, \quad (2)$$

where $\varepsilon_{eq}^p = [(2/3)\varepsilon_{ij}^p \varepsilon_{ij}^p]^{1/2}$, $\dot{\varepsilon}_{eq} = [(2/3)\dot{\varepsilon}_{ij}\dot{\varepsilon}_{ij}]^{1/2}$, $\dot{\varepsilon}_0 = 1.0\ \mathrm{s}^{-1}$, a, b, c, n, m are the material parameters, T is the temperature, $\overline{T} = (T - T_r)/(T_m - T_r)$, T_r is the room temperature, T_m is the melting temperature, k_h is the coefficient of Hall–Petch relation, and C_0, C_1, C_3, C_4, n_1 are the constants dependent on the material.

The calculations are performed for alloy E110 with an average grain size of 7 μm in the plastic strain range from 0 to 14% and the temperature range from 297 to 1173 K. The values for the parameters of the Johnson–Cook model are shown in Table 1. The values for the material parameters of the modified Zerilli–Armstrong model are shown in Table 2. T_m was assumed equal to 2130 K.

RESULTS AND DISCUSSION

Figure 1a shows the calculated stress versus equivalent plastic strain curves for uniaxial tension of Zr–1Nb–1Sn alloy (E110 analog) at a constant strain rate of 10^{-3} s^{-1}.

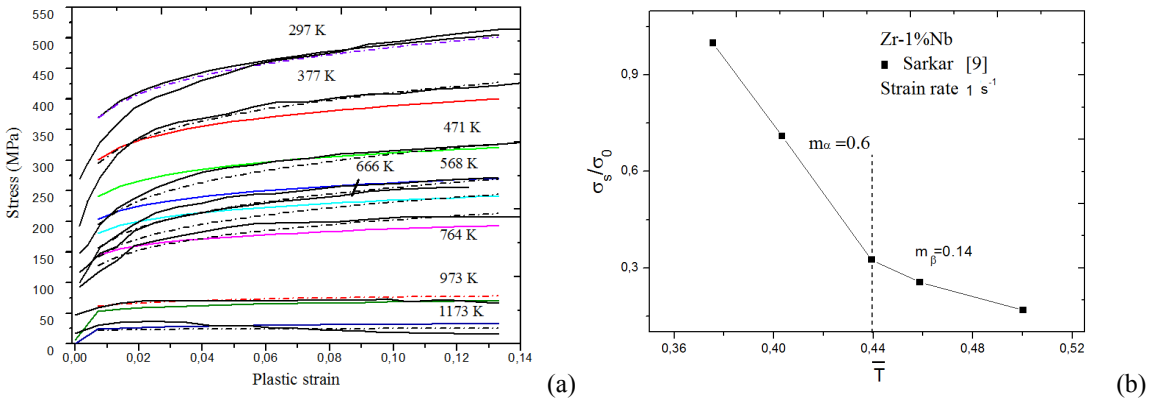

FIGURE 1. Stress versus plastic strain under uniaxial tension of Zr–1Nb–1Sn alloy at a strain rate of 10^{-3} s^{-1} (a), normalized yield strength versus normalized temperature under tension at strain rate 1 s^{-1} for Zr–1% Nb alloy (b). Symbols are experimental data [9]

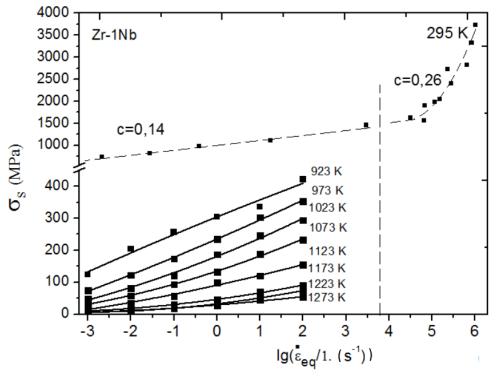

FIGURE 2. Normalized yield strength versus logarithm of normalized strain rate under tension for Zr–1Nb alloy samples. Symbols are experimental data [5, 10–12]

The solid black curves indicate experimental true stress versus true strain [3, 4]. The colored and dashed curves were obtained using Eqs. (2) and (1), respectively. The simulation results agree with experimental data within the temperature range from 297 to 1173 K. The Zerilli–Armstrong model describes the change of strain hardening in the temperature range more adequately in comparison with the Johnson–Cook model.

The dependence of the normalized yield strength of Zr–1% Nb alloy under tension with a strain rate of 1 s^{-1} on the normalized temperature $\bar{T} = (T - T_r)/(T_m - T_r)$ is shown in Fig. 1b, σ_0 is equal to $(a + k_h d_g^{-1/2})$ for the Johnson–Cook model or $(C_0 + k_h d_g^{-1/2})$ for the Zerilli–Armstrong model. The dependency change $\sigma_s/\sigma_0(\bar{T})$ at $\bar{T}$ = 0.44($T \sim$ 1070 K) is the result of a phase transition in Zr–1% Nb alloy from the alpha phase (HCP lattice) to the beta phase (BCC lattice). The numerical values of m or C_3 in the Johnson–Cook and Zerilli–Armstrong models should be refined if the temperature exceeds the onset temperature of $\alpha \rightarrow \beta$ phase transformations (~1070 K).

Figure 2 displays the simulation results for the yield strength versus the logarithm of normalized strain rate under tension of Zr–Nb. The average grain size was 15 μm. The solid curves were calculated in the temperature range from 295 to 1273 K and the strain rate range from 10^{-3} to 10^{2} s^{-1}. The dashed curve was calculated at room temperature and the strain rate range from 10^{-3} to 10^{6} s^{-1}. Experimental data [5, 9–11] are denoted by filled symbols.

Thus, it was shown that the dependence of the yield strength of Zr–1Nb alloy on the logarithm of normalized strain rate is close to linear in the temperature range from 297 to 1273 K and the strain rate range from 10^{-3} to 10^{2} s^{-1}. Both models (Zerilli–Armstrong and Johnson–Cook) allow obtaining satisfactory predictions of the yield stress under tension in the strain rate range from 10^{-3} to ~10^{3} s^{-1} and temperature from 297 to 1273 K. It was found that it is necessary to change the numerical value of the coefficient c in the Johnson-Cook model to obtain a satisfactory agreement of the calculated yield strength with experimental data [12].

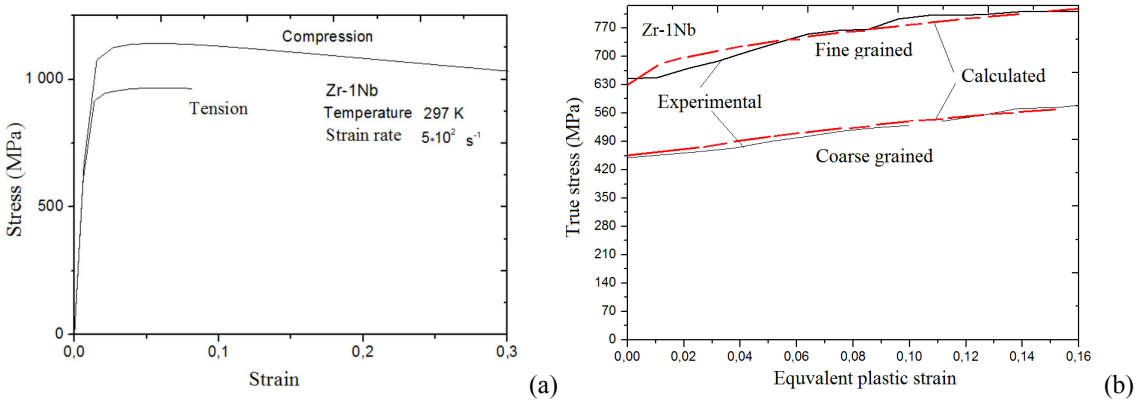

FIGURE 3. Calculated stress-strain curves of Zr–1Nb under tension and compression (a). Calculated stress versus equivalent plastic strain of UFG and CG Zr–1Nb (b). Solid curves are experimental data [6]. Dashed curves were calculated by the Zerilli–Armstrong model

The calculated stress-strain curves of Zr–1Nb under tension and compression, as well as the calculated stress versus equivalent plastic strain of UFG and CG Zr–1Nb are shown in Figs. 3a and 3b, respectively.

It is shown that the macroscopic flow stress of Zr–Nb alloys under dynamic compression and tension is different. This effect is caused by plastic flow instabilities in Zr–1Nb at the macro- and mesoscale levels under quasi-static and dynamic loads. The effects of strain hardening, thermal softening, and softening due to local damages were considered in the computational model. Different values of the yield stress were obtained in simulation of uniaxial tension and compression of plane and cylindrical alloy specimens at constant strain rates. The descending branch of the stress-strain curve under axial compression was obtained in the calculations when forming the system of shear bands. The calculated strain to fracture under compression of Zr–1Nb is higher than that under tension. The calculated stress-strain curves for CG and UFG E110 (Zr–1Nb) alloy specimens at room temperature are shown in Fig. 3b. The numerical simulation results on quasi-static loading of Zr–1Nb alloys have a good agreement with experimental data on quasi-static deformation of UFG Zr–1Nb alloys [6, 13–15]. The calculated stress-strain curves were obtained for UFG alloys taking into account changes in the coefficient k_h in comparison with the value for GC alloys.

CONCLUSIONS

The mechanical behavior of Zr–Nb alloys has been described using modified Zerilli–Armstrong and Johnson–Cook models.

The modifications of these models were proposed for the description of Zr–1Nb ultrafine- and coarse-grained alloys. The model parameters for Zr–1Nb alloy were determined.

The both models allow obtaining satisfactory predictions of the yield stress under tension within the range of strain rates from 10^{-3} to ~10^{3} s^{-1} and temperature from 297 to 1273 K.

It was shown that the flow stress of Zr–Nb alloys under compression and tension is different.

The dependence of the normalized yield strength of Zr–1Nb on normalized temperature can be approximated by a bilinear relation. The change in the curve slope is due to the $\alpha \rightarrow \beta$ phase transition (T ~ 1070 K) in Zr–Nb alloys.

ACKNOWLEDGMENTS

This work was partially supported by the Grant of the Russian Federation President MK-2690.2017.8, SP-1916.2015.2, and by a grant from the Foundation of Mendeleev National Research Tomsk State University within the Program of increasing the TSU competitiveness. The authors are grateful for the support of this research.

REFERENCES

1. D. A. Blokhin, V. M. Chernov, and A. I. Blokhin, Adv. Mater. 23–29 (2011).
2. M. A. Yilmazbayhan and M. da Silva Gomes, J. Nucl. Mater. **371**, 61–75 (2007).
3. R. W. L. Fong, J. Nucl. Mater. **440**, 467–476 (2013).
4. R. Kapoor, S. L. Wadekar, and J. K. Chakravartty, Mater. Sci. Eng. A **328**, 324–333 (2002).
5. D. Xiao, Y. Li, and S. Hu, J. Mater. Sci. Technol. **26**, 878–882 (2010).
6. E. N. Stepanova and G. P. Grabovetskaya, J. Alloys Compounds **645**, 271–274 (2015).
7. W. Zhang and Y. Cai, *Continuum Damage Mechanics and Numerical Applications* (Springer Science & Business Media, 2010).
8. S. Milani, W. Dabboussi, J. A. Nemes, and R. C. Abeyaratne, Int. J. Impact Eng. **36**, 294–302 (2009).
9. F. J. Zerilli and R. W. Armstrong, Acta Met. Mater. **40**, 1803–1808 (1992).
10. A. Sarkar, S. A. Chandanshive, and K. M. Thota, J. Alloys Compounds **703**, 56–66 (2017).
11. R. Kapoor, A. Sarkar, and J. Singh, Scripta Mater. **74**, 72–75 (2014).
12. D. N. Kazakov, O. E. Kozelkov, and A. S. Mayorova, EPJ Web Conf. **94**, 1–5 (2015).
13. D. Zou, B. Luan, and Q. Liu, Trans. Nonferrous Met. Soc. China **22**, 2402–2408 (2012).
14. C. J. Ruestes, G. Bertolino, M. Ruda, **71**, 9–12 (2014).
15. D. Guo, Z. Zhang, G. Zhang, M. Li, Y. Shi, T. Ma, and X. Zhang, Mater. Sci. Eng. A **591**, 167–172 (2014).